CHEMICAL PHYSICS

Real-time observation of water radiolysis and hydrated electron formation induced by extreme-ultraviolet pulses

Vít Svoboda[1]*, Rupert Michiels[2], Aaron C. LaForge[2], Jakub Med[3], Frank Stienkemeier[2], Petr Slavíček[3]*, Hans Jakob Wörner[1]*

The dominant pathway of radiation damage begins with the ionization of water. Thus far, however, the underlying primary processes could not be conclusively elucidated. Here, we directly study the earliest steps of extreme ultraviolet (XUV)–induced water radiolysis through one-photon excitation of large water clusters using time-resolved photoelectron imaging. Results are presented for H_2O and D_2O clusters using femtosecond pump pulses centered at 133 or 80 nm. In both excitation schemes, hydrogen or proton transfer is observed to yield a pre-hydrated electron within 30 to 60 fs, followed by its solvation in 0.3 to 1.0 ps and its decay through geminate recombination on a ~10-ps time scale. These results are interpreted by comparison with detailed multiconfigurational non-adiabatic ab-initio molecular dynamics calculations. Our results provide the first comprehensive picture of the primary steps of radiation chemistry and radiation damage and demonstrate new approaches for their study with unprecedented time resolution.

INTRODUCTION

Understanding of the primary steps of water photolysis and radiolysis remains unexpectedly humble despite the paramount importance of these processes in chemistry, biophysics, atmospheric sciences, and technology (*1*–*3*). Important processes involving the ionization of water include the damage to living matter caused by ionizing radiation, the destruction of toxic organic compounds by irradiation, and a wide range of applications in radiotherapy (*1*, *4*). The radiolysis of water leads to the extremely fast formation of various reactive particles, notably OH· radicals and hydrated electrons e^-(aq), followed by a cascade of reactions that unfolds on a broad range of time scales (*2*, *3*). The very early stages of these processes, taking place on (sub)femtosecond time scales, are poorly understood because of the lack of ultrashort extreme ultraviolet (XUV) laser pulses that would allow for their direct experimental investigation.

The hydrated electron has attracted considerable attention since its discovery by Hart and Boag in 1963 (*5*). Time-resolved studies, so far, mainly relied on charge transfer to solvent (CTTS), i.e., the photoexcitation of a solute such as I^- or organic molecules with femtosecond UV laser pulses [see, e.g., (*6*–*12*)]. Although these techniques have provided very important insights into the thermalization and solvation of electrons, they could not address their formation and early-time dynamics following water ionization. In addition, the effects of the parent particle on the dynamics of the hydrated electron may be challenging to assess. Complementary insights were obtained through multiphoton excitation of water at various central wavelengths [see, e.g., (*13*–*16*)]. Last, the study of water clusters carrying an excess electron (*2*, *17*–*21*) or deposited alkali atoms (*22*) has also provided valuable insights into the hydrated electron. Despite some controversies, e.g., concerning the binding motif of the electron or energy extrapolation from water clusters to bulk water (*9*, *10*, *12*, *15*, *19*, *20*, *22*, *23*), the thermalized hydrated electron is now well characterized experimentally (*22*–*27*).

In this study, we directly observe the birth of the hydrated electron during water radiolysis. We exploit the novel capabilities opened by femtosecond XUV laser pulses to explore the earliest stages of the ionization of water with unprecedented detail and time resolution. This work is enabled by the recent development of low-order harmonic sources based on frequency doubling of titanium:sapphire laser systems (*28*–*30*). As we show, such a radiation source enables the most direct approach to studying the ultrafast dynamics of the creation and solvation of electrons in water. In contrast to our recent work (*26*), carried out at higher photon energies at the free-electron laser FERMI, here, each water cluster absorbs at most a single XUV photon, greatly simplifying the interpretation. Compared to related work that focused on the effect of scattering on the properties of the equilibrated solvated electron (*27*), our more than 2.5 times higher time resolution uncovers the birth of the pre-hydrated electron and also reveals the decay of the solvated electron in water clusters. Our experimental results are interpreted by comparison with multiconfigurational nonadiabatic molecular dynamics (MD) calculations. This method, initially designed for computational photodynamics, is extended in our work to describe the primary stages of ultrafast radiation chemistry. The combination of experimental and theoretical results provides the first comprehensive mechanistic picture of the quantum dynamics of water radiolysis, ranging from water excitation, followed by hydrogen or proton transfer, to electron creation by autoionization, to thermalization of the hydrated electron, and lastly, to its decay via geminate recombination.

[1]Laboratory of Physical Chemistry, ETH-Zürich, 8093 Zürich, Switzerland. [2]Institute of Physics, University of Freiburg, 79104 Freiburg, Germany. [3]Department of Physical chemistry, UCT Prague, 16628 Prague, Czech Republic.
*Corresponding author. Email: vit.svoboda@phys.chem.ethz.ch (V.S.); petr.slavicek@vscht.cz (P.S.); hwoerner@ethz.ch (H.J.W.)

RESULTS AND DISCUSSION

In total, we performed four measurements using pump pulses centered at 133 and 80 nm and two water-cluster samples, H_2O and D_2O. Unless stated otherwise, a measured time-resolved

photoelectron spectrum (TRPES) of H_2O clusters excited with a 133-nm pump pulse is discussed as an example. The complementary data are shown in the Supplementary Materials. The measured TRPES is shown in Fig. 1A as a function of the vertical binding energy (VBE) and the time delay between the pump (133 nm) and probe pulses (266 nm). All TRPES display one dominant band (see section S1 for the remaining three TRPES). From previous measurements of the VBE of water anionic clusters, liquid water jets (*12*, *18*, *22*), and water clusters (*26*), the dominant feature is assigned to the prehydrated or hydrated electron. The corresponding photoelectron band appears around time zero with VBE around 2 eV and progressively shifts toward a VBE of ~3.7 eV. The intensity of the band simultaneously decreases to ~14% of its initial value within the first 10 ps.

We analyze the measured TRPES using a global-fit approach, the result of which is shown in Fig. 1B. Details of the fitting procedure are given in section S2. The global fit reproduces well all the main characteristics of the TRPES and therefore captures all important information contained in the experimental data. At very short time delays, the region of VBEs above 3 eV is dominated by a few sharp features that we assign to the Rydberg states of uncondensed water molecules. These features are identified through the global-fit procedure (see section S2) and excluded from the following analysis and discussion.

We first focus on the decay of the hydrated-electron signal, obtained by energy integration over the corresponding band. The result is shown in Fig. 1D, together with a fitted biexponential decay. The biexponential character of the signal over the observed delay range is confirmed using a logarithmic plot (see fig. S5). The maximum of the prehydrated electron signal appears at $\tau_1 = (43 \pm 7)$ fs as shown in the inset of Fig. 1D. The prehydrated electron appears as a relatively broad band centered at a VBE of 2.5 eV. The time constants of the subsequent biexponential decay are $\tau_2 = (0.44 \pm 0.05)$ ps and $\tau_3 = (8.0 \pm 1.5)$ ps.

Next, we analyze the VBE and the full width at half maximum (FWHM) of the hydrated electron band. These quantities are extracted by fitting a Gaussian function to every time slice of the hydrated electron band and are shown in Fig. 2. The VBE displays a biexponential evolution from its initial value of ~2.5 eV to its final value of (3.69 ± 0.04) eV. The FWHM of the hydrated electron band narrows in time from an initial value of ~1.8 eV to the final value of ~1 eV in the limit of large pump-probe delays. This time evolution is well represented by a monoexponential fit. We note that the TRPES are rather complex and possibly somewhat affected by the subtraction of the monomer contribution at early time delays. Details are given in sections S2 and S3. Last, we turn to the asymmetry parameter maps extracted from the time-dependent photoelectron angular distributions. The asymmetry parameter (Fig. 1C) shows little evolution as a function of time and an asymptotic value of $\beta_{2,\,lim} = (0.4 \pm 0.1)$.

Our measured data in combination with multiconfigurational nonadiabatic ab initio MD calculations provide a comprehensive view

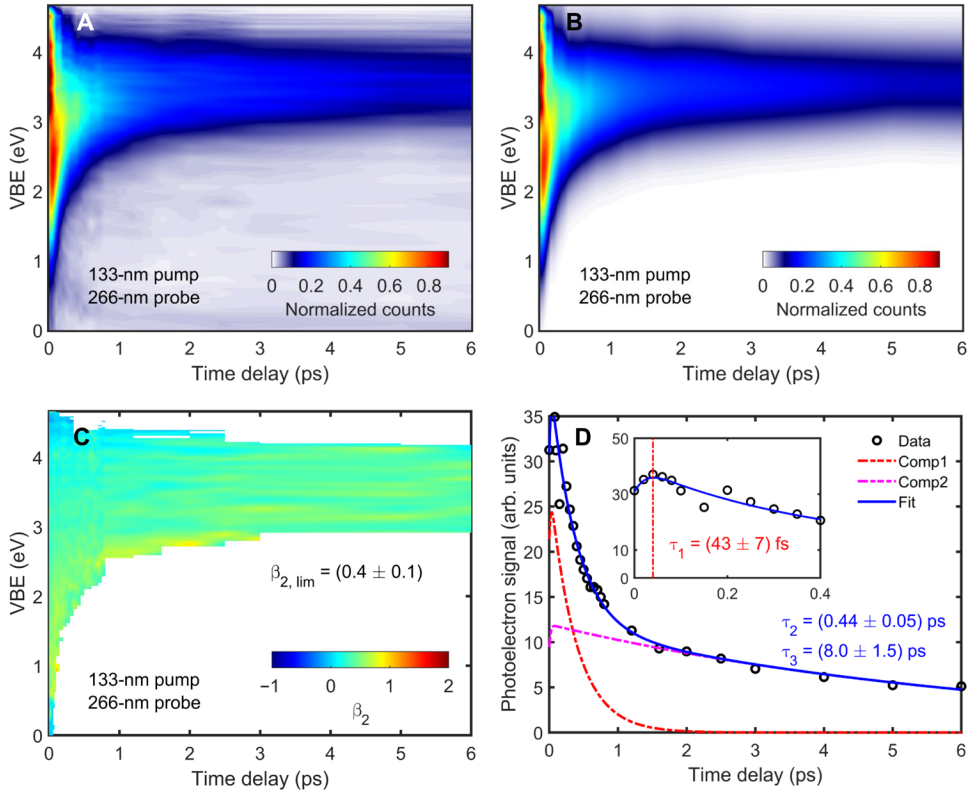

Fig. 1. Time-resolved photoelectron spectra and asymmetry parameters of the hydrated electron dynamics. (**A**) Measured TRPES of H_2O clusters pumped and probed by 133-nm and 266-nm femtosecond pulses, respectively, as a function of VBE and time delay. The normalized photoelectron counts are shown in false-color representation. (**B**) The global fit to the measured data. (**C**) Map of the asymmetry parameter β_2. (**D**) Integrated signal of the hydrated electron band as a function of time delay. The signal is fitted using a biexponential decay function (individual components are represented by the red and pink dash-dotted lines) convoluted with the laser cross-correlation function. The inset shows a zoomed area between 0 and 400 fs with a clear maximum in the signal at τ_1.

of the ionization dynamics of water and the formation of hydrated electrons. In the following, we interpret the four main results of our experiments: (i) the decay of the hydrated electron signal, (ii) the observed shift of the VBE, (iii) the narrowing of the hydrated electron band, and (iv) the evolution of the photoelectron asymmetry parameter.

When the water cluster interacts with a 133-nm pulse, corresponding to a photon energy of ~9.3 eV, direct photoionization cannot take place because the excitation energy lies below the ionization potential of water clusters of any size (*31*) and below the threshold energy for vertical ionization of liquid water (*32*). Instead, photoexcitation takes place. Excitation at photon energies above 8 eV has been predicted to result in the formation of a hydronium radical $H_3O\cdot$ and a hydroxyl radical OH· (*33*–*35*) following hydrogen atom transfer. The hydronium radical was hypothesized as the precursor of the hydrated electron (*36*). Whereas a free hydronium radical is a metastable species with a lifetime of <50 fs (*33*) in its electronic ground state, the hydrated hydronium radical can spontaneously decay into a $H_3O^+\cdots e^-$ ion pair (in analogy to the $Na^+\cdots e^-$ pair in Na-doped water clusters), which leads to the formation of a hydrated electron e^-(aq) (*33*, *37*, *38*), explaining the rapid increase in the cluster lifetime with size. It is therefore conceivable that the hydrated electron is formed via hydrogen transfer upon photoexcitation.

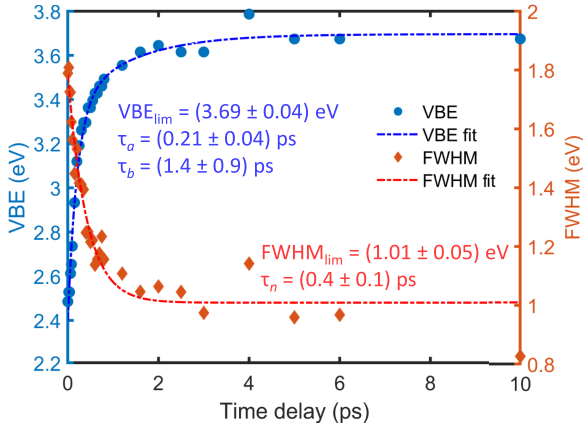

Fig. 2. Time-dependent VBE, in blue, and FWHM of the hydrated electron band, in red, shown in combination with the corresponding fits.

To test our hypothesis, we use nonadiabatic MD calculations at the complete active space self-consistent field (CASSCF) level of theory, using the computationally tractable $(H_2O)_8$ cluster as a model system. This is, to our knowledge, the first direct simulation of the hydrated electron formation during photolysis or radiolysis. We simulate the excitation of the water octamer into the second excited state (ES2) manifold (see section S5 for more details) centered at around 9.4 eV (see Fig. 3B), i.e., very close to the 133-nm (~9.3 eV) excitation wavelength used in this work. Our calculations confirm the formation of the $H_3O\cdot$ radical as shown in Fig. 3A.

We have further analyzed the character of the hydronium moiety formed upon the ultrafast hydrogen transfer: It could either be a

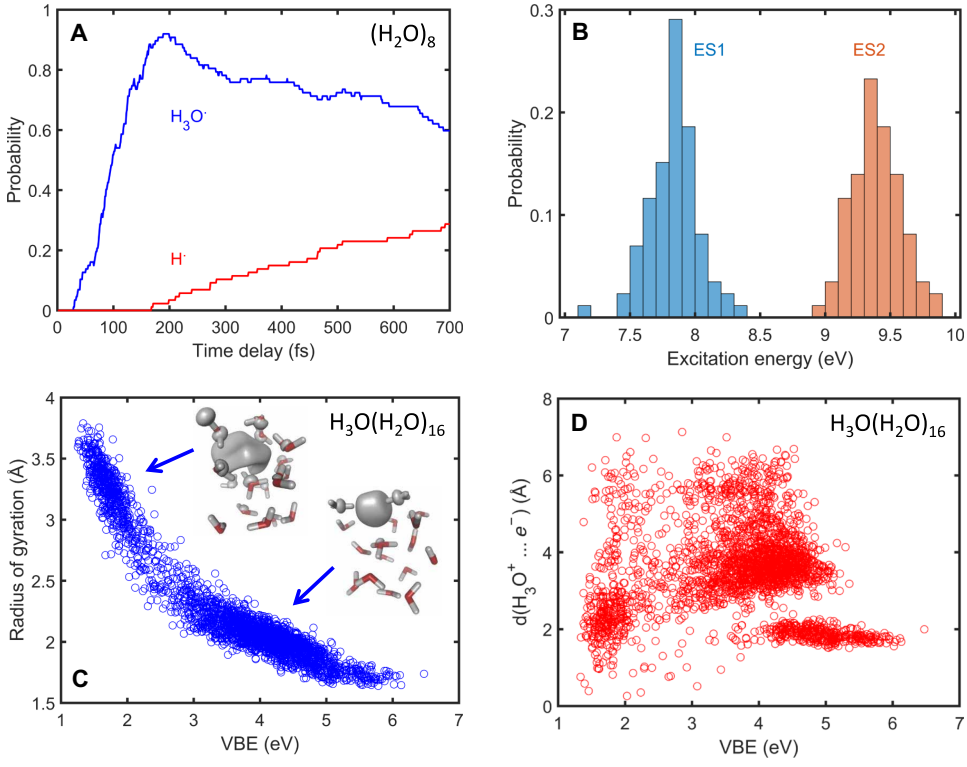

Fig. 3. Results of ab initio nonadiabatic MD calculations. (**A**) Dynamics of water octamer clusters following pulsed excitation into the second electronically excited manifold (ES2), showing the formation of hydronium radicals (blue curve), which are best interpreted as $H_3O^+\cdots e^-$, and hydrogen atoms (red curve). (**B**) Histogram of excitation energies of the first and second electronically excited manifolds (ES1 and ES2) of the initial structures of 90 unique trajectories calculated at the CASPT2(2,3)/6-31+g* level of theory. (**C** and **D**) Correlation between the radius of gyration (C) or the $H_3O^+\cdots e^-$ distance (D) and the binding energy of hydrated electron structures identified in calculations on $H_3O(H_2O)_{16}$ in the ground electronic state calculated at the density functional theory level. The insets in (C) show the spin density of the unpaired electron in $H_3O(H_2O)_{16}$ for the limiting cases of small and large radii of gyration.

valence radical or it could represent a hydronium cation H_3O^+ with a detached hydrated electron ($H_3O^+ \cdots e^-$). Population analysis in the excited state reveals that the latter description is more adequate—the hydrated electron is formed almost immediately upon hydrogen transfer ($H_2O \ldots HOH \rightarrow H_2OH \ldots OH$); the details can be found in section S6. The binding energy of the nascent electron was found to be around 1 eV, i.e., somewhat below the experimental result of ~2.5 eV, possibly due to the small cluster size amenable to our high-level calculations (see section S7 for details). At these early times after excitation, the electron is not yet equilibrated and is therefore referred to as "prehydrated" electron. In the subsequent dynamics, we expect the electron to gradually thermalize and the system to relax into its electronic ground state.

We also observe the gradual formation of hydrogen atoms during the simulation (red curve in Fig. 3A). On the basis of the above-mentioned analysis, this is the signature of the recombination of the hydrated electron with an H_3O^+ cation, forming H + H_2O, and represents the most likely mechanism of the hydrated electron decay observed in our experiments. Our calculations predict a time scale of hundreds of femtoseconds for this decay in photoexcited $(H_2O)_8$, whereas our experiments reveal a much slower time scale of 8.0 to 11.2 ps. These rather different time scales are consistent with the strong size dependence of the hydronium cation concentration of the respective cluster sizes.

This decrease in the geminate recombination rate with increasing cluster size is also consistent with the ejection length of ~1.4 nm and the longer recombination times known from bulk studies using two-photon excitation at 266 nm, i.e., the same excitation energy (*32*). Although geminate recombination in bulk water is known to have a nonexponential time dependence, a biexponential fit to the data presented in (*32*) yields a very reasonable agreement with fast time constants of 23.5 and 24.8 ps and slow time constants of 340 and 390 ps for bulk H_2O and D_2O that were two-photon excited at 266 nm, respectively. The faster time constants therefore agree with our results, keeping in mind that the ejection length is similar to the cluster radius (~1.4 nm; see Methods), and the ejection length might even be shorter for one-photon excitation at 133 nm since it decreases from ~2.4 nm for three-photon excitation at 400 nm (*16*) to ~1.4 nm for two-photon excitation at 266 nm. The slower time constants are not observable within the delay range covered by our experiments.

The water octamer for which nonadiabatic first-principle dynamics calculations are computationally affordable is too small to allow for the observation of the complete equilibration of the hydrated electron. We have therefore modeled larger clusters composed of the relevant H_3O moiety and 16 water molecules in their electronic ground state. These simulations characterize the thermalized hydrated electron, as we expect it to be prepared in our experiments. In particular, we have calculated the VBEs of the $H_3O(H_2O)_{16}$ system. Depending on the initial structure of the water cluster, we identified a broad variety of hydrated electron structures with VBEs ranging from 1.3 to 6.1 eV. Figure 3C reveals the existence of a direct relationship between the binding energy and the radius of gyration, i.e., the effective size of the hydrated electron cloud. A similar relationship was previously established in the case of excess electrons in anionic water clusters [see (*3*) for a review] or in isoelectronic sodium-doped neutral water clusters (*39*). These structures with compact electron clouds were found to have high VBEs, whereas the more delocalized electron clouds correspond to lower VBEs. In contrast to these results, the distance between the center of the electron cloud and the hydronium cation does not seem to have an important effect on the VBE (Fig. 3D). On the basis of these results, we assign our observations of a time-dependent increase in the VBE to an increasing localization of the hydrated electron within the water clusters during the solvation process.

Our results for all four experiments are summarized in Table 1 and in sections S3 to S5. Our experimental results reveal the formation of a single, Gaussian-shaped hydrated electron band, corresponding to a VBE of (3.69 ± 0.04) eV. The higher signal-to-noise ratio of our results (see fig. S4, B to D) compared to (*27*) excludes a possible bimodal distribution of the hydrated electron, in agreement with a recent viewpoint (*40*) that identified it as an artifact based on incorrect assumptions. Compared to measurements on anionic water clusters, this observation would be consistent with the formation of a "cavity" isomer (*20*), but our own calculations show that clusters as small as $H_3O(H_2O)_{16}$ can display an average VBE of 3.6 eV (Fig. 3C), demonstrating a pronounced difference between hydrated electrons in neutral and anionic water clusters. In our earlier study of hydrated electrons in overall neutral water clusters (*26*), we have shown that the VBE does not depend on cluster size for average sizes between 250 and 2200. The solvated electron in overall neutral clusters therefore shares more similarities with that in Na-doped water clusters, which are also neutral as a whole and are stabilized by a Coulomb interaction between the cation and the hydrated electron, than with anionic water clusters. In addition, the Na-doped clusters are isoelectronic to the clusters studied in our work. Hence, it is expected that our

Table 1. Time constants determined from measurements on H_2O and D_2O water clusters. The decays are analyzed in terms of a biexponential function (τ_2 and τ_3), with a time origin shifted by τ_1, convoluted with the experimental cross-correlation function. The VBE is fitted with a biexponential function to obtain time constants (τ_a and τ_b). Similarly, the time evolution of the FWHM is fitted with a monoexponential function to obtain time constant τ_n. Values of $FWHM_{lim}$ are obtained by a Gaussian fit to time slices at 10 ps.

	τ_1 (fs)	τ_2 (ps)	τ_3 (ps)	τ_a (ps)	τ_b (ps)	τ_n (ps)	VBE_{lim} (eV)	$FWHM_{lim}$ (eV)
				H_2O				
133 nm	43 ± 7	0.44 ± 0.05	8.0 ± 1.5	0.21 ± 0.04	1.4 ± 0.9	0.4 ± 0.1	3.69 ± 0.04	1.01 ± 0.05
80 nm	26 ± 6	0.37 ± 0.04	10.9 ± 4.3	0.18 ± 0.03	1.3 ± 0.9	0.7 ± 0.2	3.71 ± 0.04	0.85 ± 0.06
				D_2O				
133 nm	61 ± 6	1.0 ± 0.3	9.3 ± 4.0	0.21 ± 0.02	1.8 ± 0.7	1.3 ± 0.3	3.63 ± 0.06	0.96 ± 0.05
80 nm	65 ± 6	0.6 ± 0.1	11.2 ± 3.2	0.18 ± 0.02	1.7 ± 0.6	1.2 ± 0.6	3.69 ± 0.03	0.9 ± 0.1

results agree well with the known properties of these clusters (*22*, *39*). Moreover, the VBE of Na-doped water clusters converge to the bulk value for sizes as small as four to five water molecules, which is also in agreement with our present and earlier (*26*) results.

The delayed maximum of the (pre)hydrated electron signal (τ_1) occurring at 26 to 43 fs in H_2O and 61 to 65 fs in D_2O clusters is attributed to hydrogen or proton transfer in case of 133- or 80-nm excitation path, respectively. This assignment is in agreement with the observed isotope effect and with the proton transfer dynamics in ionized liquid water (*41*). This transfer is the first step in a reaction chain, which leads to a highly excited, hot electron. What follows is the solvation of this prehydrated electron with a time constant τ_2, which again displays a pronounced isotope effect, in agreement with the involvement of solvent rearrangement, which is expected to mainly involve librational modes (*15*, *19*). The solvation process is accompanied by a gradually increasing localization that translates into the observed increase in the VBE. The fast time constant (τ_a) displays no isotope effect within the accuracy of our results, whereas the slower one (τ_b) may display a weak isotope effect. The narrowing of the VBE distribution, which occurs with the time constant τ_n and is assigned to the cooling of the initially hot prehydrated electron, does display an isotope effect, at least following the excitation at 133 nm.

The shortest time scale (τ_1), which we have assigned to hydrogen/proton transfer (43/26 fs in H_2O and 61/65 fs in D_2O), has not been observed in previous experiments, which studied either excess electrons or electrons created through CTTS or used multiphoton excitation of neat water. It has also not been reported in prior measurements on neutral water clusters (*26*, *27*) because of insufficient time resolution. The second shortest time scale (τ_2), which we assigned to solvation dynamics (0.37/0.44 ps in H_2O and 1.0/0.6 ps in D_2O), is in reasonable agreement with the 0.3 ps obtained by Paik *et al.* (*19*) as the solvation time in the electronic ground state following internal conversion of an excess electron in anionic water clusters $[(H_2O)_n^-$ with $n = 15$ to 35]. This time scale is also very similar to that observed in bulk liquid water (*15*). These time scales are also consistent with the solvation time constants determined for small iodide-doped water clusters (*42*), which amounted to 0.39 ps for $I^-(D_2O)_5$, 0.47 fs for $I^-(H_2O)_5$, and 0.56 ps for $I^-(D_2O)_6$.

Last, we return to the photoelectron asymmetry parameters. Compared to previous experiments on the s → p photoexcitation of initially equilibrated hydrated electrons in liquid microjets (*12*), which showed a decay of the asymmetry parameter from 0.16 to 0 assigned to the p → s internal conversion, our experiments may suggest a direct relaxation of the hydrated electron to the s ground state (see Fig. 1C). This interpretation also agrees with the lack of anisotropy in the terahertz absorption of the solvated electron, reported in (*16*).

These combined experimental and theoretical results are schematically summarized in Fig. 4. The excitation path initiated by 133-nm irradiation prepares a highly excited water molecule H_2O^* in the cluster environment. The hydrated H_2O^* molecule undergoes a rapid hydrogen-transfer reaction with a neighboring water molecule yielding a highly excited hydrated hydronium radical $H_3O\cdot$. In the next step, the hydronium radical decays in a spontaneous charge separation process into a hydrated hydronium cation H_3O^+ and a prehydrated electron e^-(aq). The prehydrated electron then thermalizes with its environment and localizes. Recombination of the hydrated electron with the parent hydrated hydronium cation H_3O^+ results in the formation of a hydrated water molecule and a hydrogen atom, which is ejected from the cluster (*33*–*35*).

In contrast to this, 80-nm irradiation results either in excitation of quasi-bound states, which derive from the Rydberg states converging to the first or second excited states of H_2O^+ (superexcited states) or in the direct ionization of the water cluster because the photon energy is higher than the first ionization energy of water clusters of all sizes (*31*). The superexcitation pathway leads to a similar situation as in the case of 133-nm excitation (see Fig. 4) (*32*). The ionization step can be followed by an ultrafast proton transfer yielding an H_3O^+ cation and a prehydrated electron (*43*). Thermalization of this electron yields the hydrated electron e^-(aq). As in the

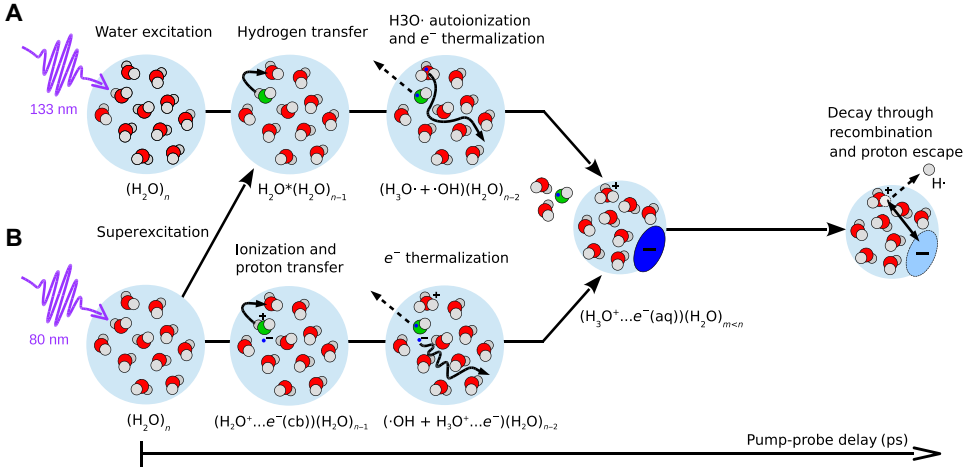

Fig. 4. Schematic representation of the XUV-induced radiolysis of a water cluster and hydrated electron formation. (**A**) The 133-nm irradiation creates a highly excited water molecule H_2O^*, highlighted in green, which undergoes hydrogen atom transfer yielding a hydronium radical $H_3O\cdot$. This radical decays to form a hydrated electron e^-(aq), simultaneously with a hydroxyl radical OH·. (**B**) The water cluster is irradiated by the 80-nm pulse leading to either superexcitation or direct ionization. The superexcitation path is similar to the 133-nm irradiation. The ionization path creates an electron e^-(cb) in the conduction band and an ionized water molecule H_2O^+. Next, a proton transfer happens giving H_2O^+ + OH·. The initially hot electron is thermalized and lastly forms a hydrated electron e^-(aq). During thermalization, several water molecules and a hydroxyl radical OH· are ejected from the cluster. In both cases, the hydrated electron is detected with a 266-nm probe pulse. The signal of the hydrated electron decays in time due to a recombination reaction between H_3O^+ and the hydrated electron, which leads to a hydrogen atom escaping from the cluster.

previous case, the hydrated electron can recombine with H_3O^+, as shown in Fig. 4B. The similarity of these two mechanisms offers an explanation for the similarity of the observed time scales following the two excitation pathways.

CONCLUSION

In this work, we have combined the advantages of low-order harmonic generation with time-resolved velocity map imaging (VMI), to observe the early time scales involved in the excitation and subsequent hydration dynamics in water clusters. Our observations reveal the entire pathway from the electronic excitation, followed by hydrogen/proton transfer and the formation of a prehydrated electron to its subsequent thermalization, spatial localization, and its eventual decay through geminate recombination. We have performed four complementary measurements, investigating the role of the excitation/ionization energy and the isotope effects. We have observed unexpected similarities between the two pathways. Combining experimental and theoretical results, we have found that the two excitation pathways only differ in the creation step of the electron. The observed dynamics are generally slower in D_2O clusters, signaling the important contributions of structural dynamics to the observed processes. Our results uncover the mechanisms triggered by the ionization of water with unprecedented detail, including the nature and time scales of the individual quantum-mechanical processes. These results have important implications for the understanding of the primary steps of radiation chemistry and radiation damage. They also demonstrate a pathway for studying such dynamics with even higher, attosecond, temporal resolution by either combining two neighboring harmonic orders into an attosecond pulse train and performing an interferometric measurement, as demonstrated on gaseous (*44*) and liquid water (*45*) or using isolated attosecond pulses in the vacuum UV/XUV domain.

METHODS

Experiment

All experiments were performed using a two-color pump-probe scheme using low-order harmonic generation in a semi-infinite gas cell and a VMI spectrometer (*30*), as shown in Fig. 5. A Ti:Sa regenerative amplifier operating at 1 kHz delivered 2.0-mJ pulses centered at 800 nm with 28-fs pulse duration. The input beam was divided into a pump and a probe arm using a 80:20 beam splitter. The transmitted (pump) beam was delayed with respect to the reflected beam (probe) using a motorized delay stage. The transmitted beam was frequency doubled using a 300-μm-thick β-barium borate crystal to obtain 570-μJ pulses at 400 nm. The second harmonic beam was separated from the fundamental beam by reflections on four dichroic mirrors and focused by a $f = 500$-mm spherical mirror into the semi-infinite gas cell filled with Xe. The pressure of the generation gas was selected such that the third (133 nm ~ 9.3 eV) or fifth (80 nm ~ 15.5 eV) harmonic of 400 nm was optimized. Under these conditions no photoelectrons originating from the other harmonics were detected. The reflected beam was used for the third harmonic generation giving 1.2-μJ pulses of 266 nm. Both pump and probe beams were delivered into a vacuum chamber using dichroic mirrors and then focused noncollinearly (with a crossing angle of less than 1°), by two spherical mirrors ($f = 0.5$ m for harmonics and $f = 1$ m for 266 nm). All in-vacuum mirrors were motorized allowing for fine adjustment of the spatial overlap.

Purified water with an electrical resistivity of 18 MΩ was held in a heatable reservoir. The reservoir temperature was set to 170°C corresponding to a water backing pressure of about 8 bar. The reservoir was connected to a CRUCS pulsed valve through individually heatable in-vacuum and out-vacuum tubes, all kept at 190°C. The pulsed nozzle (orifice, 150 μm; half-opening angle, 40°) was kept at 188°C. All temperatures were stabilized to better than ±3°C. These conditions provided water clusters with an average

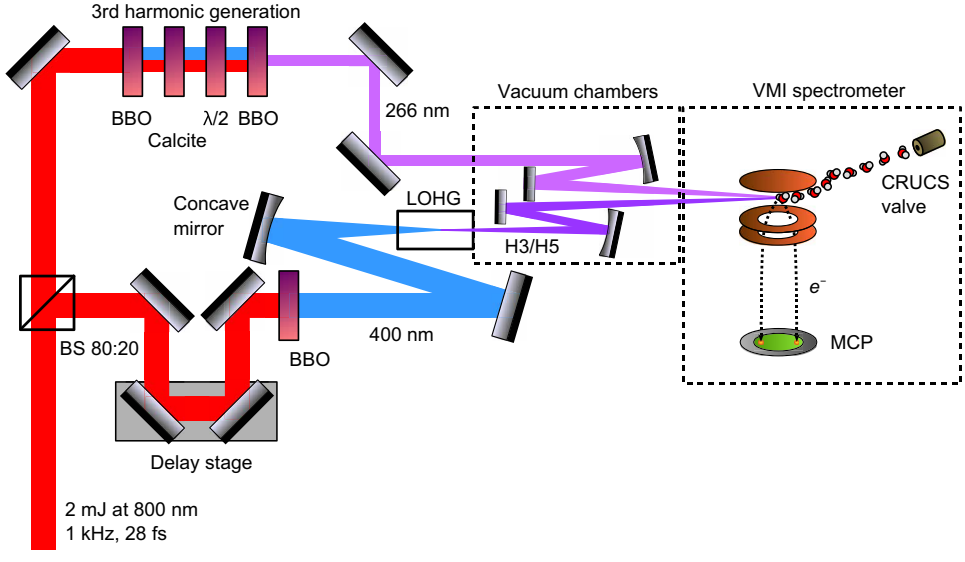

Fig. 5. The experimental setup consists of a femtosecond pump-probe beamline and a VMI spectrometer. A Ti:Sa regenerative amplifier delivers 28-fs pulses at a 1-kHz repetition rate with 2.0-mJ energy. The input pulse is split by an 80:20 beam splitter (BS) into a pump and a probe arm. The reflected part is frequency doubled, separated from its fundamental by reflection on dichroic mirrors and used to generate low-order harmonics in a semi-infinite gas cell (LOHG). The transmitted part is used in third harmonic generation process to obtain 266-nm probe pulses that are separated from the fundamental and 400 nm beams by dichroic mirrors. Both beams are noncollinearly overlapped in the interaction region of the VMI spectrometer using motorized mirrors. The sample is delivered by a CRUCS pulsed valve and intersected with beams in the interaction region. Photoelectrons are extracted by electrostatic lenses and detected by a position sensitive detector (MCP, micro channel plate).

cluster size of $\langle N \rangle \approx 400$ water molecules estimated using a formula derived in (*46*). Assuming a spherical shape and the density of liquid water, the average cluster size would correspond to a radius of ~1.4 nm, but we note that these clusters usually have highly nonspherical shapes (*47*).

The pulsed nozzle was operated at 500 Hz. The gas jet was skimmed by a 500-μm skimmer and propagated 10-cm downstream to reach the interaction region where it was ionized by the combined action of the laser beams. A cross-correlation of (85 ± 3) fs (FWHM) was determined by two-color ionization (133 + 266 nm) of Xe. The cross-correlation function was taken into account during data analysis as an instrument response function. Ejected photoelectrons were imaged using electrostatic lenses fulfilling VMI conditions and a microchannel plate (MCP) detector in a chevron configuration.

TRPES were recorded for pump-probe delays between −0.3 and +10.0 ps. The negative delays refer to the situation where the 266-nm pulse acts as the pump. At each time step of the TRPES, the following four images were recorded: (i) one two-color image, (ii) two one-color images (where one of the two beams was blocked), and (iii) one background image. Each image was recorded three times over 2.5×10^4 laser shots. One-color data were then subtracted from the two-color data to obtain images of the pump-probe contributions. These images were inverted using polar Onion peeling inversion and Maximum Entropy Velocity Image Reconstruction methods. Calibration of the energy axis was performed using Xe and Kr measurements recorded under the same VMI conditions.

Theory

The excited-state ab-initio MD simulations were executed with the surface hopping approach using Tully's fewest switches algorithm. We used a water octamer as a model system. The dynamics were performed on the CASSCF potential energy surface, using a rather restricted active space consisting of two electrons in three orbitals. The system was promoted either into the ES1 or into the ES2 manifold of states. Simulations with larger active spaces and number of states, as well as simulations of smaller systems (trimer), provided qualitatively similar results. The equations of motion were integrated with the velocity Verlet integrator, using a timestep of 10 atomic units (a.u.). The initial geometries were generated by classical MD simulations using hybrid PBE0 functional with Grimme's D3 dispersion correction. A constant temperature of 200 K was maintained by Nosé-Hoover thermostat. The equations of motion during the ground-state simulations were integrated with the velocity Verlet integrator, using a timestep of 20 a.u.

The possible states of hydrated electron in the $H_3O(H_2O)_n$ clusters in thermal equilibrium were investigated by means of MD simulations. We considered clusters with $n = 4$, 8, 12, and 16. In all cases, we ran simulations for 10 ps at a temperature of 200 K maintained by Nosé-Hoover thermostat. The PBE functional with 6-31+g* basis set was used to calculate forces and velocities for all the calculations. The equations of motion were integrated with the velocity Verlet integrator. We recalculated ionization energies and radii of gyration along the trajectory with the long-range corrected (LC)–ωPBE functional.

The MOLPRO package was used for calculating the energies and forces, and the graphics processing unit–based TeraChem code was used for the calculations in the ground state. The ionization energies were calculated with Gaussian 09 code. All MD simulations were performed within our in-house code ABIN.

SUPPLEMENTARY MATERIALS

Supplementary material for this article is available at http://advances.sciencemag.org/cgi/content/full/6/3/eaaz0385/DC1

Section S1. Measured TRPES
Section S2. Analysis of the data—Extraction of the hydrated electron signal
Section S3. Detailed analysis of the hydrated electron signal
Section S4. Photoelectron angular distributions
Section S5. Wave functions of the excited water octamer during the dynamics
Section S6. Charge distribution on different electronic states along the excited trajectories
Section S7. Ionization energies of different electronic states along the excited trajectories
Fig. S1. All four measured TRPES.
Fig. S2. Comparison between cluster and monomer TRPES.
Fig. S3. The results of the slice analysis demonstrated on the TRPES for H_2O clusters excited by a 133-nm pulse.
Fig. S4. Four experimental spectra (blue circles) at time delays of 0.06, 0.5, 2, and 6 ps, respectively.
Fig. S5. Integrated signal of the hydrated electron band as a function of the time delay.
Fig. S6. Hydrated electron dynamics are analyzed in detail by means of two measures: (i) the shift in the vertical binding energies (VBE), in blue, and (ii) the band narrowing, in red, represented as a decrease in the FWHM of the hydrated electron band.
Fig. S7. Angular-resolved photoelectron distributions from the velocity map imaging of the water clusters represented by the anisotropy parameter β_2.
Fig. S8. Visualization of involved molecular orbitals.
Fig. S9. Charge distributions.
Fig. S10. Ionization energies of different electronic states.

REFERENCES AND NOTES

1. B. C. Garrett, D. A. Dixon, D. M. Camaioni, D. M. Chipman, M. A. Johnson, C. D. Jonah, G. A. Kimmel, J. H. Miller, T. N. Rescigno, P. J. Rossky, S. S. Xantheas, S. D. Colson, A. H. Laufer, D. Ray, P. F. Barbara, D. M. Bartels, K. H. Becker Jr., S. E. Bradforth, I. Carmichael, J. V. Coe, L. R. Corrales, J. P. Cowin, M. Dupuis, K. B. Eisenthal, J. A. Franz, M. S. Gutowski, K. D. Jordan, B. D. Kay, J. A. LaVerne, S. V. Lymar, T. E. Madey, C. W. McCurdy, D. Meisel, S. Mukamel, A. R. Nilsson, T. M. Orlando, N. G. Petrik, S. M. Pimblott, J. R. Rustad, G. K. Schenter, S. J. Singer, A. Tokmakoff, L.-S. Wang, C. Wettig, T. S. Zwier, Role of water in electron-initiated processes and radical chemistry: Issues and scientific advances. *Chem. Rev.* **105**, 355–390 (2005).
2. R. M. Young, D. M. Neumark, Dynamics of solvated electrons in clusters. *Chem. Rev.* **112**, 5553–5577 (2012).
3. J. M. Herbert, M. P. Coons, The hydrated electron. *Annu. Rev. Phys. Chem.* **68**, 447–472 (2017).
4. D. M. Bartels, D. Gosztola, C. D. Jonah, Spur decay kinetics of the solvated electron in heavy water radiolysis. *J. Phys. Chem. A* **105**, 8069–8072 (2001).
5. J. W. Boag, E. J. Hart, Absorption spectra in irradiated water and some solutions: Absorption spectra of 'hydrated' electron. *Nature* **197**, 45–47 (1963).
6. Y. Kimura, J. C. Alfano, P. K. Walhout, P. F. Barbara, Ultrafast transient absorption spectroscopy of the solvated electron in water. *J. Phys. Chem.* **98**, 3450–3458 (1994).
7. A. Baltuška, M. F. Emde, M. S. Pshenichnikov, D. A. Wiersma, Early-time dynamics of the photoexcited hydrated electron. *J. Phys. Chem. A* **103**, 10065–10082 (1999).
8. S. E. Bradforth, P. Jungwirth, Excited states of iodide anions in water: A comparison of the electronic structure in clusters and in bulk solution. *J. Phys. Chem. A* **106**, 1286–1298 (2002).
9. A. Lübcke, F. Buchner, N. Heine, I. V. Hertel, T. Schultz, Time-resolved photoelectron spectroscopy of solvated electrons in aqueous NaI solution. *Phys. Chem. Chem. Phys.* **12**, 14629–14634 (2010).
10. M. H. Elkins, H. L. Williams, A. T. Shreve, D. M. Neumark, Relaxation mechanism of the hydrated electron. *Science* **342**, 1496–1499 (2013).
11. F. Messina, O. Bräm, A. Cannizzo, M. Chergui, Real-time observation of the charge transfer to solvent dynamics. *Nat. Commun.* **4**, 2119 (2013).
12. S. Karashima, Y.-i. Yamamoto, T. Suzuki, Resolving nonadiabatic dynamics of hydrated electrons using ultrafast photoemission anisotropy. *Phys. Rev. Lett.* **116**, 137601 (2016).
13. R. A. Crowell, D. M. Bartels, Multiphoton ionization of liquid water with 3.0–5.0 eV photons. *J. Phys. Chem.* **100**, 17940–17949 (1996).
14. J. A. Kloepfer, V. H. Vilchiz, V. A. Lenchenkov, A. C. Germaine, S. E. Bradforth, The ejection distribution of solvated electrons generated by the one-photon photodetachment of aqueous I^- and two-photon ionization of the solvent. *J. Chem. Phys.* **113**, 6288–6307 (2000).
15. P. Kambhampati, D. H. Son, T. W. Kee, P. F. Barbara, Solvation dynamics of the hydrated electron depends on its initial degree of electron delocalization. *J. Phys. Chem. A* **106**, 2374–2378 (2002).
16. J. Savolainen, F. Uhlig, S. Ahmed, P. Hamm, P. Jungwirth, Direct observation of the collapse of the delocalized excess electron in water. *Nat. Chem.* **6**, 697–701 (2014).

17. G. H. Lee, S. T. Arnold, J. G. Eaton, H. W. Sarkas, K. H. Bowen, C. Ludewigt, H. Haberland, Negative ion photoelectron spectroscopy of solvated electron cluster anions, $(H_2O)_n^-$ and $(NH_3)_n^-$. *Z. Phys. D Atoms Mol. Clusters* **20**, 9–12 (1991).
18. A. E. Bragg, J. R. Verlet, A. Kammrath, O. Cheshnovsky, D. M. Neumark, Hydrated electron dynamics: From clusters to bulk. *Science* **306**, 669–671 (2004).
19. D. H. Paik, I.-R. Lee, D.-S. Yang, J. S. Baskin, A. H. Zewail, Electrons in finite-sized water cavities: Hydration dynamics observed in real time. *Science* **306**, 672–675 (2004).
20. J. R. R. Verlet, A. E. Bragg, A. Kammrath, O. Cheshnovsky, D. M. Neumark, Observation of large water-cluster anions with surface-bound excess electrons. *Science* **307**, 93–96 (2005).
21. L. Ma, K. Majer, F. Chirot, B. von Issendorff, Low temperature photoelectron spectra of water cluster anions. *J. Chem. Phys.* **131**, 144303 (2009).
22. B. Abel, U. Buck, A. L. Sobolewski, W. Domcke, On the nature and signatures of the solvated electron in water. *Phys. Chem. Chem. Phys.* **14**, 22–34 (2012).
23. K. R. Siefermann, Y. Liu, E. Lugovoy, O. Link, M. Faubel, U. Buck, B. Winter, B. Abel, Binding energies, lifetimes and implications of bulk and interface solvated electrons in water. *Nat. Chem.* **2**, 274–279 (2010).
24. A. Kumar, J. A. Walker, D. M. Bartels, M. D. Sevilla, A simple ab initio model for the hydrated electron that matches experiment. *J. Phys. Chem. A* **119**, 9148–9159 (2015).
25. C.-C. Zho, B. J. Schwartz, Time-resolved photoelectron spectroscopy of the hydrated electron: Comparing cavity and noncavity models to experiment. *J. Phys. Chem. B.* **120**, 12604–12614 (2016).
26. A. C. LaForge, R. Michiels, M. Bohlen, C. Callegari, A. Clark, A. von Conta, M. Coreno, M. Di Fraia, M. Drabbels, M. Huppert, P. Finetti, J. Ma, M. Mudrich, V. Oliver, O. Plekan, K. C. Prince, M. Shcherbinin, S. Stranges, V. Svoboda, H. J. Wörner, F. Stienkemeier, Real-time dynamics of the formation of hydrated electrons upon irradiation of water clusters with extreme ultraviolet light. *Phys. Rev. Lett.* **122**, 133001 (2019).
27. T. E. Gartmann, L. Ban, B. L. Yoder, S. Hartweg, E. Chasovskikh, R. Signorell, Relaxation dynamics and genuine properties of the solvated electron in neutral water clusters. *J. Phys. Chem. Lett.* **10**, 4777–4782 (2019).
28. R. Rajeev, J. Hellwagner, A. Schumacher, I. Jordan, M. Huppert, A. Tehlar, B. R. Niraghatam, D. Baykusheva, N. Lin, A. von Conta, H. J. Wörner, In situ frequency gating and beam splitting of vacuum- and extreme-ultraviolet pulses. *Light: Sci. Appl.* **5**, e16170 (2016).
29. J. L. Ellis, D. D. Hickstein, W. Xiong, F. Dollar, B. B. Palm, K. E. Keister, K. M. Dorney, C. Ding, T. Fan, M. B. Wilker, K. J. Schnitzenbaumer, G. Dukovic, J. L. Jimenez, H. C. Kapteyn, M. M. Murnane, Materials properties and solvated electron dynamics of isolated nanoparticles and nanodroplets probed with ultrafast extreme ultraviolet beams. *J. Phys. Chem. Lett.* **7**, 609–615 (2016).
30. V. Svoboda, N. B. Ram, R. Rajeev, H. J. Wörner, Time-resolved photoelectron imaging with a femtosecond vacuum-ultraviolet light source: Dynamics in the $\widetilde{A}/\widetilde{B}$ - and $\widetilde{F}$ -bands of SO_2. *J. Chem. Phys.* **146**, 084301 (2017).
31. L. Belau, K. R. Wilson, S. R. Leone, M. Ahmed, Vacuum ultraviolet (VUV) photoionization of small water clusters. *J. Phys. Chem. A* **111**, 10075–10083 (2007).
32. C. G. Elles, I. A. Shkrob, R. A. Crowell, S. E. Bradforth, Excited state dynamics of liquid water: Insight from the dissociation reaction following two-photon excitation. *J. Chem. Phys.* **126**, 164503 (2007).
33. M. Ončák, P. Slavíček, M. Fárník, U. Buck, Photochemistry of hydrogen halides on water clusters: Simulations of electronic spectra and photodynamics, and comparison with photodissociation experiments. *J. Phys. Chem. A* **115**, 6155–6168 (2011).
34. V. Poterya, M. Fárník, M. Ončák, P. Slavíček, Water photodissociation in free ice nanoparticles at 243 nm and 193 nm. *Phys. Chem. Chem. Phys.* **10**, 4835–4842 (2008).
35. V. Poterya, J. Fedor, A. Pysanenko, O. Tkáč, J. Lengyel, M. Ončák, P. Slavíček, M. Fárník, Photochemistry of HI on argon and waternanoparticles: Hydronium radical generation in $HI{\cdot}(H_2O)_n$. *Phys. Chem. Chem. Phys.* **13**, 2250–2258 (2011).
36. A. L. Sobolewski, W. Domcke, Hydrated hydronium: A cluster model of the solvated electron? *Phys. Chem. Chem. Phys.* **4**, 4–10 (2002).
37. V. Poterya, O. Tkáč, J. Fedor, M. Fárník, P. Slavíček, U. Buck, Mass spectrometry of hydrogen bonded clusters of heterocyclic molecules: Electron ionization vs. photoionization. *Int. J. Mass Spectrom.* **290**, 85–93 (2010).
38. J. Ma, U. Schmidhammer, M. Mostafavi, Direct evidence for transient pair formation between a solvated electron and H_3O^+ observed by picosecond pulse radiolysis. *J. Phys. Chem. Lett.* **5**, 2219–2223 (2014).
39. C. W. Dierking, F. Zurheide, T. Zeuch, J. Med, S. Parez, P. Slavíček, Revealing isomerism in sodium-water clusters: Photoionization spectra of $Na(H_2O)_n$ (n = 2–90). *J. Chem. Phys.* **146**, 244303 (2017).
40. D. M. Bartels, Is the hydrated electron vertical detachment genuinely bimodal? *J. Phys. Chem. Lett.* **10**, 4910–4913 (2019).
41. O. Marsalek, C. G. Elles, P. A. Pieniazek, E. Pluhařová, J. VandeVondele, S. E. Bradforth, P. Jungwirth, Chasing charge localization and chemical reactivity following photoionization in liquid water. *J. Chem. Phys.* **135**, 224510 (2011).
42. L. Lehr, M. T. Zanni, C. Frischkorn, R. Weinkauf, D. M. Neumark, Electron solvation in finite systems: Femtosecond dynamics of iodide-(water)$_n$ anion clusters. *Science* **284**, 635–638 (1999).
43. O. Svoboda, D. Hollas, M. Ončák, P. Slavíček, Reaction selectivity in an ionized water dimer: Nonadiabatic ab initio dynamics simulations. *Phys. Chem. Chem. Phys.* **15**, 11531–11542 (2013).
44. M. Huppert, I. Jordan, D. Baykusheva, A. von Conta, H. J. Wörner, Attosecond delays in molecular photoionization. *Phys. Rev. Lett.* **117**, 093001 (2016).
45. I. Jordan, M. Huppert, M. A. Brown, J. A. van Bokhoven, H. J. Wörner, Photoelectron spectrometer for attosecond spectroscopy of liquids and gases. *Rev. Sci. Instrum.* **86**, 123905 (2015).
46. M. Fárník, J. Lengyel, Mass spectrometry of aerosol particle analogues in molecular beam experiments. *Mass Spectrom. Rev.* , 630–651 (2017).
47. J. Lengyel, A. Pysanenko, V. Poterya, P. Slavíček, M. Fárník, J. Kočišek, J. Fedor, Irregular shapes of water clusters generated in supersonic expansions. *Phys. Rev. Lett.* **112**, 113401 (2014).

Acknowledgments

Funding: V.S. and H.J.W. acknowledge funding from ETH-Zürich and an ERC Starting Grant (#307270-ATTOSCOPE). A.C.L. acknowledges the support of the Carl-Zeiss-Stiftung. P.S. and J.M. acknowledge the support of Czech Science Foundation, project number 18-23756S. R.M. and F.S. acknowledge the support of Deutsche Forschungsgemeinschaft project DFG STI 125/19-1. **Author contributions:** V.S. conducted the experiments with the help of R.M. and A.C.L. V.S. analyzed the data. J.M. and P.S. performed all the calculations. All authors contributed to the interpretation of the data. V.S., P.S., and H.J.W. wrote the first draft of the paper, which was improved through contributions from all authors. **Competing interests:** The authors declare that they have no competing interests. **Data and materials availability:** All data needed to evaluate the conclusions in the paper are present in the paper and/or the Supplementary Materials. Additional data related to this paper may be requested from the authors.

Submitted 7 August 2019
Accepted 26 November 2019
Published 17 January 2020
10.1126/sciadv.aaz0385

Citation: V. Svoboda, R. Michiels, A. C. LaForge, J. Med, F. Stienkemeier, P. Slavíček, H. J. Wörner, Real-time observation of water radiolysis and hydrated electron formation induced by extreme-ultraviolet pulses. *Sci. Adv.* **6**, eaaz0385 (2020).

Science Advances

Real-time observation of water radiolysis and hydrated electron formation induced by extreme-ultraviolet pulses

Vít Svoboda, Rupert Michiels, Aaron C. LaForge, Jakub Med, Frank Stienkemeier, Petr Slavícek and Hans Jakob Wörner

Sci Adv **6** (3), eaaz0385.
DOI: 10.1126/sciadv.aaz0385